η	p 0.005	0.025	0.05	0.95	0.975	0.995
1	0.00004	0.0010	0.0039	3.8415	5.0239	7.8794
1.5	0.0015	0.0131	0.0332	4.9802	6.2758	9.3310
2	0.0100	0.0506	0.1026	5.9915	7.3778	10.5966
2.5	0.0321	0.1186	0.2108	6.9281	8.3923	11.7538
3	0.0717	0.2158	0.3518	7.8147	9.3484	12.8382
3.5	0.1301	0.3389	0.5201	8.6651	10.2621	13.8696
4	0.2070	0.4844	0.7107	9.4877	11.1433	14.8603
4.5	0.3013	0.6494	0.9201	10.2882	11.9985	15.8183
5	0.4117	0.8312	1.1455	11.0705	12.8325	16.7496
5.5	0.5370	1.0278	1.3845	11.8376	13.6486	17.6583
6	0.6757	1.2373	1.6354	12.5916	14.4494	18.5476
6.5	0.8268	1.4584	1.8967	13.3343	15.2369	19.4201
7	0.9893	1.6899	2.1673	14.0671	16.0128	20.2777
7.5	1.1621	1.9306	2.4463	14.7912	16.7783	21.1222
$\Phi^{-1}(p)$	−2.5758	−1.9600	−1.6449	1.6449	1.9600	2.5758

Table 263. Percentage points $Q_\eta(p)$ for χ^2_η distribution for $\eta = 1$ to 7.5 in steps of 0.5. The bottom row gives percentage points $\Phi^{-1}(p)$ for the standard Gaussian distribution.

	$c = 1$	$c = 2$	$c = 3$	$c = 4$
$r = 0$	2.5216281	−4.7715359	7.9199915	−11.9769211
$r = 1$	16.0778828	−20.6343346	25.0531521	−28.8738136
$r = 2$	31.8046265	−34.0071373	34.7700272	−34.3151321
$r = 3$	32.7861099	−30.2861233	26.7109356	−22.8838310
$r = 4$	18.7432098	−14.5717688	10.7177744	−7.5322194
$r = 5$	4.7226319	−2.6807923	1.3391306	−0.5167125

Table 272. Coefficients $\{\phi_{24,n} : n = 1, \ldots, 24\}$ for AR(24) process (Gao, 1997). The coefficient in row r and column c is $\phi_{24,4r+c}$. These coefficients are available on the Web site for this book (see page *xiv*).

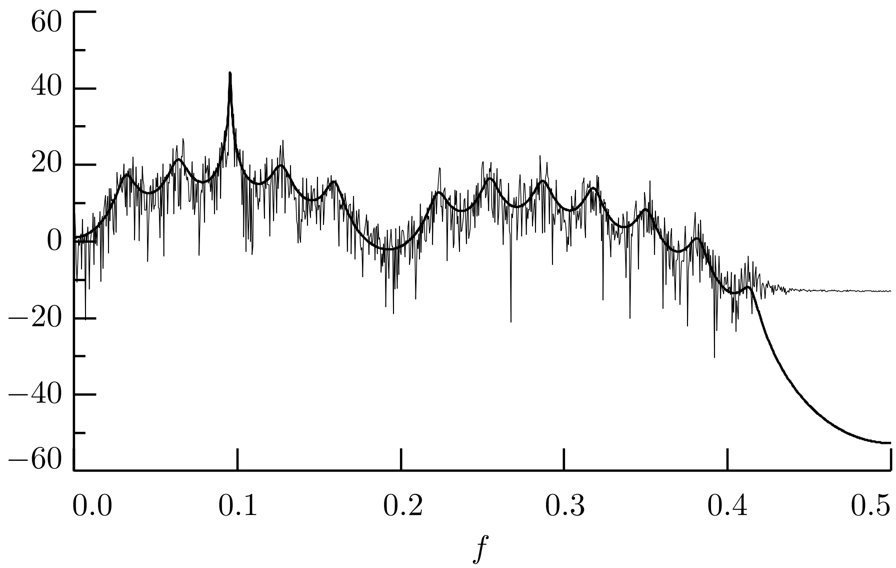

Figure 273. Periodogram (thin jagged curve) and true SDF (thick smooth) for a time series of length $N = 2048$ that is a realization of an AR(24) process (see Table 272 for the coefficients defining this process). Both the periodogram and true SDF are plotted on a decibel (dB) scale. Leakage is evident here in the periodogram at high frequencies, where the bias becomes as large as 40 dB (i.e., four orders of magnitude).

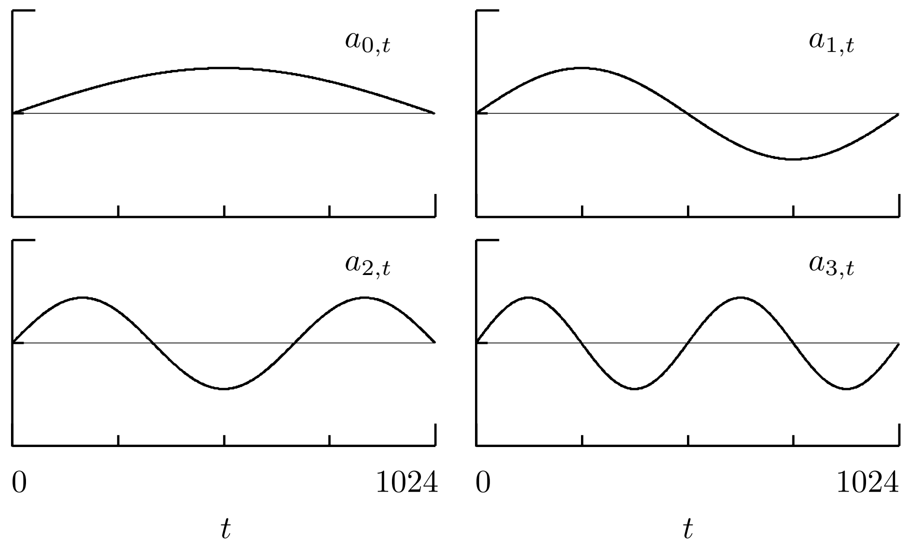

Figure 274. Sine tapers $\{a_{n,t}\}$ of orders $n = 0, 1, 2$ and 3 for $N = 1024$.

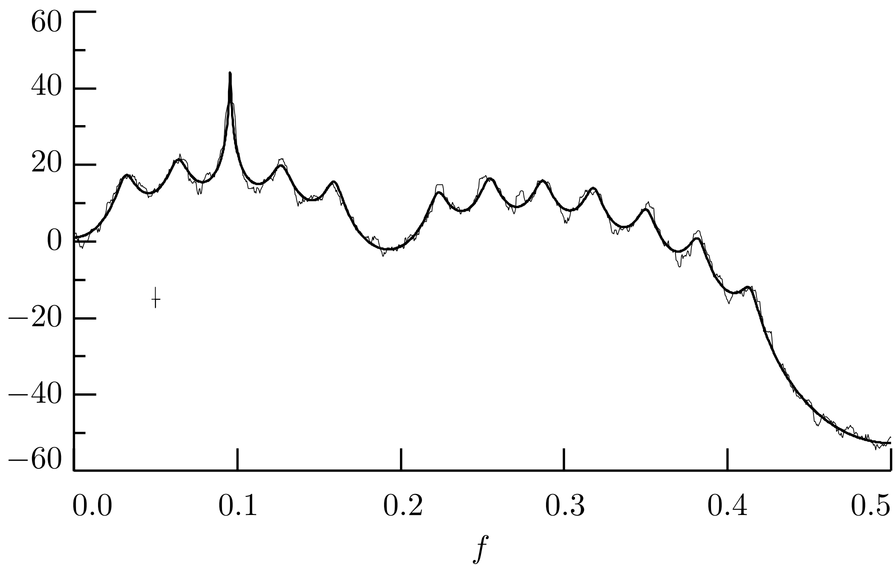

Figure 275. Multitaper SDF estimate $\hat{S}_X^{(\mathrm{mt})}(\cdot)$ (thin jagged curve) and true SDF (thick smooth) for a simulated AR(24) time series of length $N = 2048$ (the corresponding periodogram is shown in Figure 273). The multitaper estimate is based on $K = 10$ sine tapers. Both $\hat{S}_X^{(\mathrm{mt})}(\cdot)$ and the true SDF are plotted on a decibel scale. The width of the crisscross in the left-hand portion of the plot gives the bandwidth of $\hat{S}_X^{(\mathrm{mt})}(\cdot)$ (i.e., $\frac{K+1}{(N+1)} \doteq 0.0054$), while its height gives the length of a 95% confidence interval for a given $10 \cdot \log_{10}(S_X(f))$.

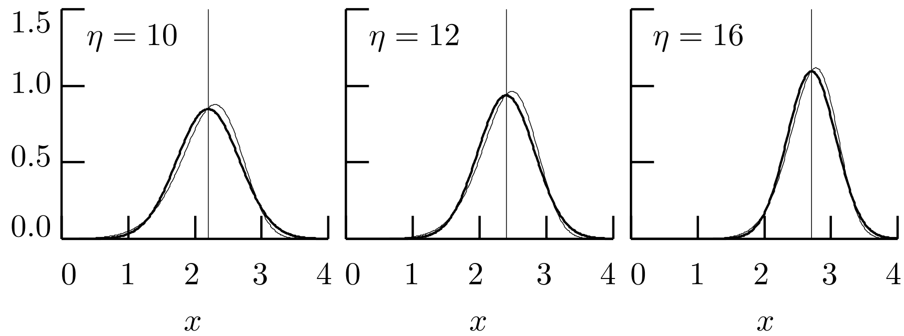

Figure 276. PDFs for $\log(\chi^2_\eta)$ RVs (thin curves) compared to Gaussian PDFs (thick curves) having the same means and variances. The degrees of freedom η are, from left to right, 10, 12 and 16 (these would be the degrees of freedom associated with a multitaper SDF estimator $\hat{S}^{(\mathrm{mt})}_X(\cdot)$ formed from, respectively, $K = 5$, 6 and 8 data tapers). The vertical lines indicate the means for the $\log(\chi^2_\eta)$ RVs – from left to right, these are $\psi(5) + \log(2) \doteq 2.199$, $\psi(6) + \log(2) \doteq 2.399$ and $\psi(8) + \log(2) \doteq 2.709$. The square roots of the corresponding variances are, respectively, $\sqrt{\psi'(5)} \doteq 0.470$, $\sqrt{\psi'(6)} \doteq 0.426$ and $\sqrt{\psi'(8)} \doteq 0.365$. (Exercise [7.1] concerns the derivation of the $\log(\chi^2_\eta)$ PDF.)

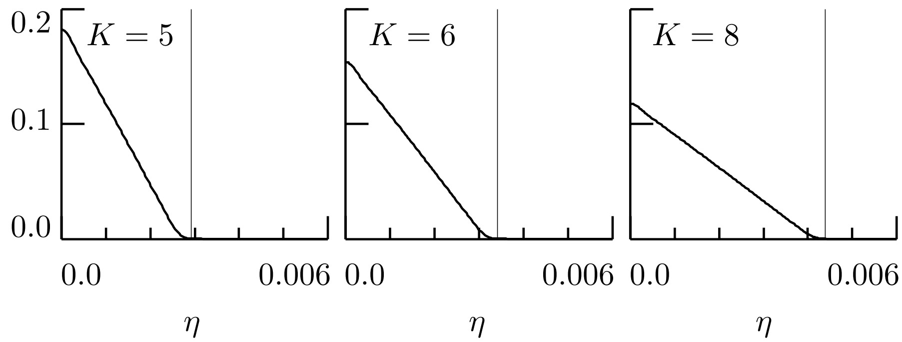

Figure 277. The autocovariance $\tilde{s}_\eta(\nu)$ versus ν for $N = 2048$ and $K = 5, 6$ and 8 sine tapers. Each vertical line shows the bandwidth $\frac{K+1}{N+1}$ of the associated multitaper SDF estimator.

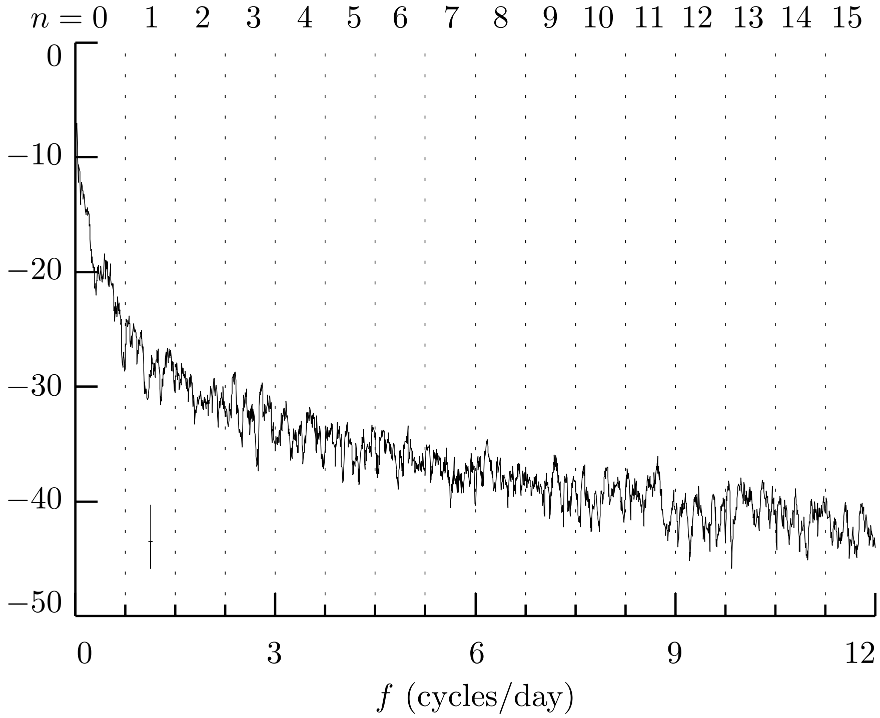

Figure 278. Multitaper SDF estimate $\hat{S}_X^{(\mathrm{mt})}(\cdot)$ (in decibels) of the solar physics time series using $K = 10$ sine tapers (this series of $N = 4096$ values is plotted in Figures 222 and 235). The vertical dotted lines partition the frequency interval $[0, 12$ cycles/day$]$ into 16 subintervals, the same as would be achieved by a level $j = 4$ DWPT (see Figures 220) or MODWPT (Figure 236). The width of the crisscross in the lower left-hand corner of the plot gives the physical bandwidth of $\hat{S}_X^{(\mathrm{mt})}(\cdot)$ (i.e., $\frac{K+1}{(N+1)\,\Delta t} \doteq 0.0644$ cycles/day – here $\Delta t = 1/24$ days), while its height gives the length of a 95% confidence interval for a given $10 \cdot \log_{10}(S_X(f))$.

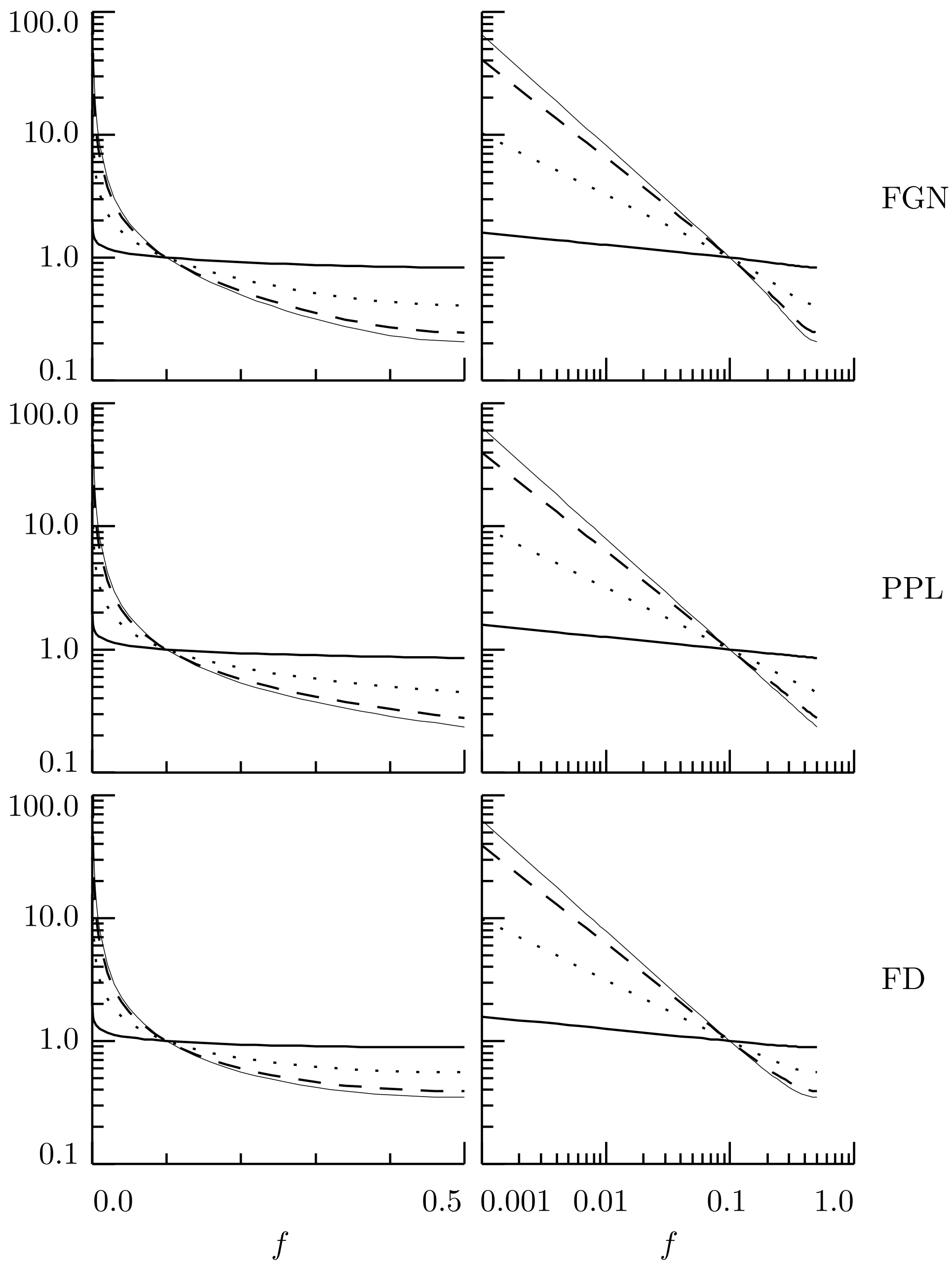

Figure 282. SDFs for FGN, PPL and FD processes (top to bottom rows, respectively) on both linear/log and log/log axes (left- and right-hand columns, respectively). Each SDF $S_X(\cdot)$ is normalized such that $S_X(0.1) = 1$. The table below gives the parameter values for the various plotted curves.

process	thick solid	dotted	dashed	thin solid
FGN	$H = 0.55$	$H = 0.75$	$H = 0.90$	$H = 0.95$
PPL	$\alpha = -0.1$	$\alpha = -0.5$	$\alpha = -0.8$	$\alpha = -0.9$
FD	$\delta = 0.05$	$\delta = 0.25$	$\delta = 0.40$	$\delta = 0.45$

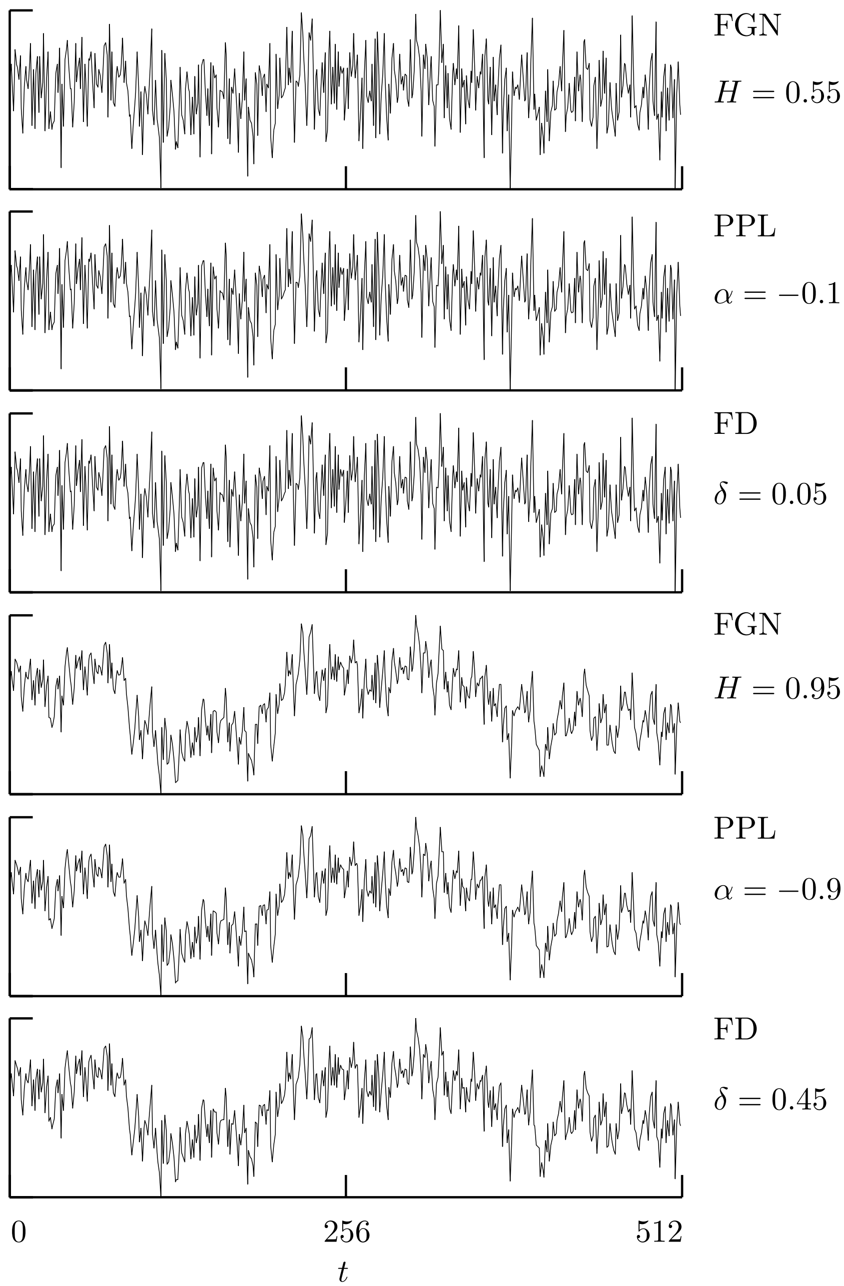

Figure 283. Simulated realizations of FGN, PPL and FD processes. The thick (thin) solid curves in Figure 282 show the SDFs for the top (bottom) three series – these SDFs differ markedly only at high frequencies. We formed each simulated $X_0, \ldots, X_{511}$ using the Davies–Harte method (see Section 7.8), which does so by transforming a realization of a portion $Z_0, \ldots, Z_{1023}$ of a white noise process (the Z_t values are on the Web site for this book – see page *xiv*). To illustrate the similarity of FGN, PPL and FD processes with comparable H, α and δ, we used the same Z_t to create all six series. Although the top (bottom) three series appear to be identical, estimates of their SDFs show high frequency differences consistent with their theoretical SDFs.

process	nonstationary LMP	stationary LMP	white noise	stationary not LMP
FGN	—	$\frac{1}{2} < H < 1$	$H = \frac{1}{2}$	$0 < H \leq \frac{1}{2}$
PPL	$\alpha \leq -1$	$-1 < \alpha < 0$	$\alpha = 0$	$\alpha \geq 0$
FD	$\delta \geq \frac{1}{2}$	$0 < \delta < \frac{1}{2}$	$\delta = 0$	$\delta \leq 0$

Table 286. Parameter ranges for each named stochastic process for which the form of the process is (a) nonstationary long memory, (b) stationary long memory, (c) white noise or (d) stationary but not long memory.

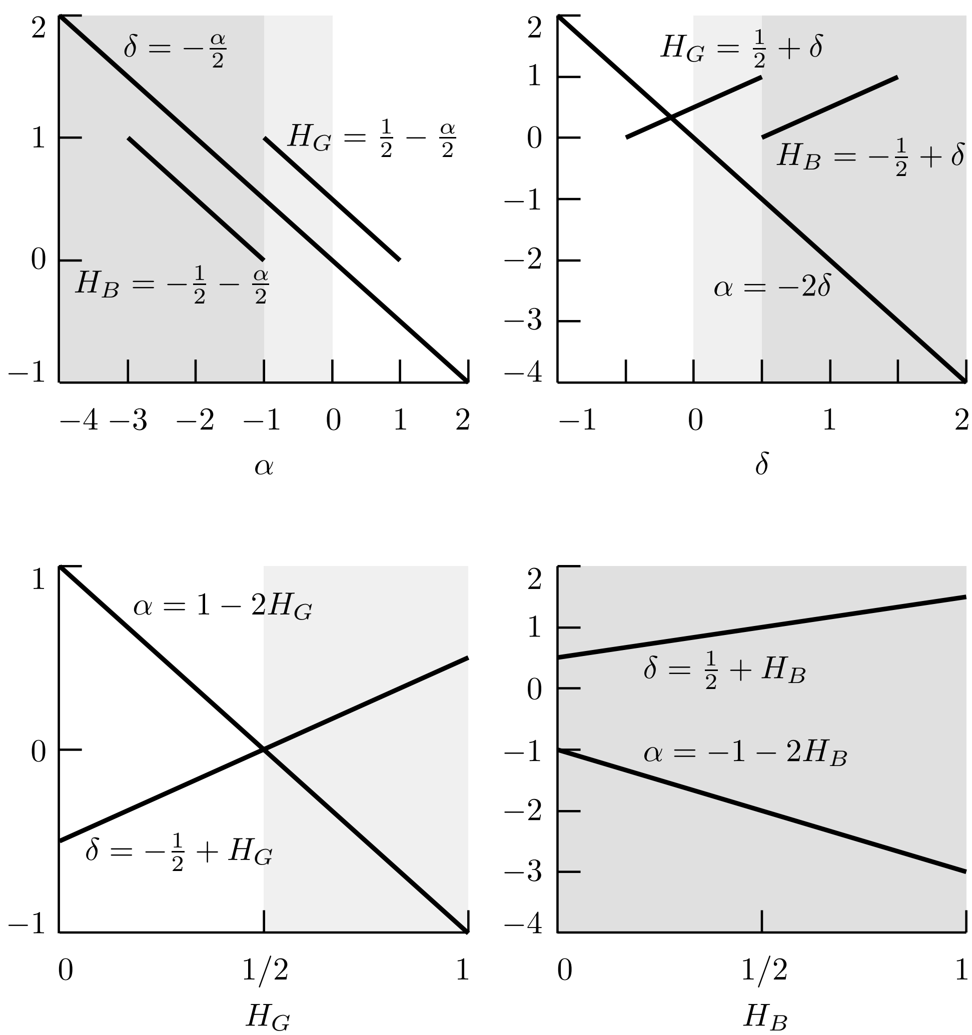

Figure 286. Relationships amongst the spectral slope α, the fractional difference parameter δ and the Hurst coefficient H (both for FGN and DFBM). The unshaded, lightly shaded and heavily shaded regions represent parameter values corresponding to, respectively, stationary processes without long memory, stationary long memory processes and nonstationary long memory processes (white noise processes occur when the boundary between the unshaded and lightly shaded regions crosses a thick line). For this plot only, we distinguish between H as a parameter for DFBM and for FGN by using H_B in the former case and H_G in the latter. Note that, while α and δ range over the entire real axis, we must have $0 < H < 1$ for both DFBM and FGN.

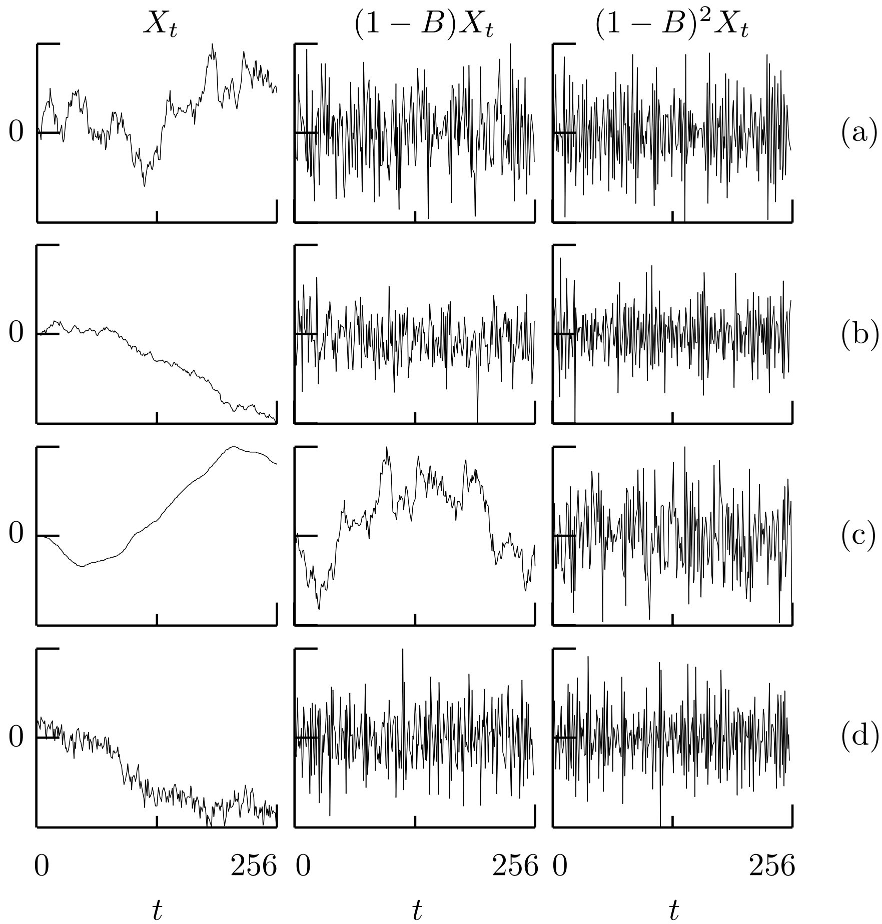

Figure 289. Simulated realizations of nonstationary processes $\{X_t\}$ with stationary backward differences of various orders (first column) along with their first backward differences $\{(1-B)X_t\}$ (second column) and second backward differences $\{(1-B)^2X_t\}$ (final column). From top to bottom, the processes are (a) a random walk; (b) a modified random walk, formed using a white noise sequence with mean $\mu_\varepsilon = -0.2$; (c) a random run; and (d) a process formed by summing the line given by $-0.05t$ and a simulation of a stationary FD process with $\delta = 0.45$.